Article

Solvent Effects on the Elasticity of Electrospinnable Polymer Solutions

Elena Ewaldz, Joshua Randrup, and Blair Brettmann*

Read Online

ACCESS | Metrics & More | Article Recommendations | Supporting Information

ABSTRACT: Ultrafine fibers manufactured through electrospinning are a frontrunner for advanced fiber applications, but transitioning from potential to commercial applications for ultrafine fibers requires a better understanding of the behavior of polymer solutions in electrospinning to enable the design of more complex spinning dopes. In complex fluids, there are viscoelastic stresses and microstructural transitions that alter free surface flows. These may not be seen in shear rheology; therefore, an in-depth analysis of the extensional rheological behavior must be performed. In this work, we use dripping-onto-substrate rheometry to characterize the extensional viscosities of electrospinning dopes from four polymer solutions commonly used in electrospinning (low- and high-molecular-weight polyvinylpyrrolidone in methanol and water as well as poly(ethylene oxide) and poly(vinyl alcohol) in water). We link the electrospinnability, characterized through fiber morphology, to the extensional rheological properties for semidilute and entangled polymer solutions and show that high-surface-tension solvents require higher extensional viscosities and relaxation times to form smooth fibers and that the Deborah and Ohnesorge numbers are a promising method of determining electrospinnability. Through this tie between solvent characteristics, viscoelasticity, and electrospinnability, we will enable the design of more complex spinning dopes amenable to applications in wearable electronics, pharmaceuticals, and more.

KEYWORDS: Electrospinning, extensional rheology, ultrafine fibers, capillary instabilities
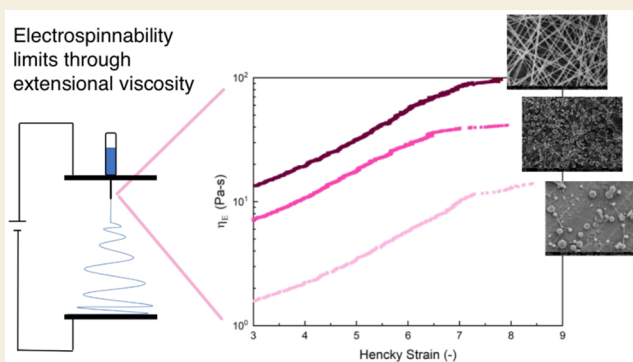
1. INTRODUCTION

Ultrafine fibers, those with a diameter less than approximately 5 μm, play a starring role in new product research in the fiber and textile industry, both for conventional textiles such as clothing and furnishing[1−4] and for technical textiles in electronics,[5,6] bioengineering,[7−10] sensors,[11−13] and more. Nevertheless, the commercial market for ultrafine fibers is still primarily limited to filtration and biomedical scaffolds, missing important application areas such as electronics, sensors, and consumer products. Advancing into these areas will broaden the polymer and additive types used and thus will require a greater variety of solvents for the spinning dopes, which will affect the fiber formation process. Traditional, large-scale fiber spinning methods, such as wet spinning, dry spinning, and melt spinning are typically only affected by large changes in fluid flow properties;[14−19] however, ultrafine fiber spinning methods such as electrospinning exhibit significant fiber formation changes in response to small changes in fluid properties such as viscosity, conductivity, elasticity, and surface tension.[20−22] Therefore, the scientific challenge of relating chemical composition to processing in multicomponent mixtures must be thoroughly addressed to enable expansion of ultrafine fiber manufacturing into these more advanced fiber applications.

The frontrunner in manufacturing technology for ultrafine fibers is electrospinning, a technology similar to dry spinning in conventional fiber production but where the pulling force is provided by an electric field, rather than mechanical intervention. Due to its relatively low productivity and high cost, electrospinning is most attractive for high-value-add products such as cell growth scaffolds,[9,10,23] pharmaceutical products,[24−26] and electronics.[13,27] Yet, high-value-add products typically come with high-performance demands and complex product specifications. To efficiently bring new products to market, a comprehensive fundamental understanding of how the solution properties affect electrospinning must be available. The current understanding of electrospinnability is derived from previous studies on simple polymer

solutions,[28−34] but there are significant knowledge gaps for how the material properties impact the viscoelastic behavior under conditions similar to those experienced in the electrospinning process, namely the high levels of elongational flow and fluid extension.

In electrospinning, typically three distinct regimes are observed when varying the solution properties and processing parameters; droplets, beads-on-string, and uniform fibers. The electrospinning process begins with a Taylor cone formed from competing electric stress on a droplet of the polymer solution and surface tension.[35] When the electric stress overcomes the surface tension, a thin jet of solution is emitted and undergoes three main modes of instabilities: two driven by electrostatic repulsion (axisymmetric and nonaxisymmetric) and one by the Rayleigh instability.[36,37] It is the Rayleigh instability that leads to capillary breakup, and it is driven primarily by the fluid's surface tension. In order to reduce the surface energy, fluids break up into droplets to minimize the total surface area. The Rayleigh instability can be stabilized and even suppressed for certain length scales through viscoelastic stresses inherent in entangled polymer solutions.[38] This leads to the three regimes of fiber morphology: droplets, beads-on-string, and uniform fibers. When there is too little viscoelasticity to resist deformation from surface tension, droplets are produced, also known as electrospraying. The next regime has a morphology of beads connected by a thin filament, and this beads-on-string structure is attributed to the partial stabilization of fibers between droplets arising from the entangled polymer networks that resist capillary breakup driven by the Rayleigh instability.[38] The third regime exhibits uniform fibers when the Rayleigh instability is sufficiently suppressed for the length scales associated with fiber formation. Therefore, the electrospinnability of polymer solutions is thought to be primarily determined by the surface tension and viscoelasticity.[39]

Much of the previous work on understanding viscoelastic effects on electrospinnability has used shear viscosity, especially zero-shear viscosity, to understand chain entanglement effects[40,41] and intermolecular interactions.[21,22] Since the polymer solution undergoes elongational flow and extension during electrospinning, extensional rheology provides superior parameters for predicting electrospinnability.[42] Previously, extensional rheological characterization of electrospinning solutions has used polymer solutions such as poly(ethylene oxide) (PEO) in aqueous solutions,[42,43] poly(methyl methacrylate) in DMF,[21,44] and nylon 6 in formic acid.[45] These studies do not consider lower-surface-tension solvents nor do they analyze more than one polymer/solvent system. This is understandable, as classic capillary breakup extensional rheometery (CaBER) is not sensitive enough for low-viscosity or weakly elastic fluids. A recent study by Khandavalli et al. utilizes dripping-onto-substrate (DoS) rheometry, which is similar to CaBER but more sensitive for low-viscosity fluids, to correlate extensional rheological parameters to the electrospinnability. While they show that the surface tension of solvents exhibits a strong influence on extensibility and fiber formation, they do not provide general insight into chemical composition effects such as the nature of the polymer and solvent.[46] Here, we investigate the strong effect of solvent surface tension on fiber formation through elasticity studies using DoS extensional rheology, which deduces that high-surface-tension solutions require significantly higher elasticity to promote smooth fiber formation. Through this tie between

solvent characteristics, viscoelasticity, and electrospinnability, we will enable the design of more complex spinning solutions amenable to applications in wearable electronics, pharmaceuticals, and more.

2. METHODS

2.1. Materials

All polymers and solvents were used as received. Polyvinylpyrrolidone (PVP) (M_w = 1300 and 55 kg/mol) was purchased from Millipore Sigma. Poly(ethylene oxide) (PEO) (M_w = 1000 kg/mol) was purchased from Alfa Aesar. Poly(vinyl alcohol) (PVA) (M_w = 145−180 kg/mol, 88% hydrolyzed) was purchased from Acros Organics. Polymer structures are shown in Figure 1.
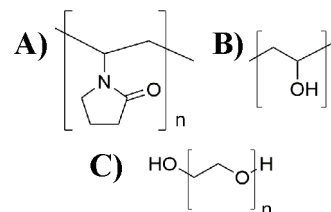

Figure 1. Chemical structures of polymers used in study. (A) PVP, (B) PVA, (C) PEO.

Certified ACS reagent grade methanol (MeOH) was purchased from Fisher Chemical. Deionized water (18.2 MΩ cm) was obtained from a Milli-Q system. Reagent grade Triton X-100 was purchased from VWR. Solutions were prepared in varying concentrations (w/w) by combining the polymer with the designated solvent and mixing using a magnetic stirrer overnight. We were not able to use all polymers in both solvents due to the poor solubility of PEO and PVA in MeOH.

2.2. Procedures

2.2.1. Surface Tension. Surface tension values for the selected concentrations for each polymer system were evaluated from 10 points spaced 0.5 s apart using the pendant drop method on a goniometer (Ramé Hart Model 250). The values were obtained through DropImage Advanced software. At least 10 different droplets for each concentration were evaluated.

2.2.2. Shear Rheology. Zero-shear viscosity (η_0) measurements were obtained using a rheometer (TA Instruments DHR-3) with a double-gap cylinder geometry. The measurements were taken at 25 °C using a shear rate sweep spanning at least two decades between 0.1 and 1000 s^{-1} depending on the solution viscosity for best resolution. The η_0 values were found by averaging the plateau region as the shear rate approached zero.

2.2.3. Extensional Rheology. Extensional rheology of the fluids was characterized using DoS, which was pioneered by Dinic et al.[47] DoS allows analysis of the capillary thinning and pinch-off dynamics for low-viscosity and more weakly viscoelastic fluids than typically evaluated in capillary breakup extensional rheometry (CaBER). In DoS, an elongated liquid bridge is formed between a substrate and a sessile drop from a nozzle. The optimal distance between the nozzle and substrate is about 3 times the diameter of the nozzle. The diameter of the nozzle used was 1.55 mm, and the flow rate was set to 1 mL/h. Videos of the thinning capillary bridge were captured at a frame rate of 8000−10 000 fps using a high-speed camera (Chronos 1.4) with a 12.5−75 mm f/1.2 zoom lens and super macro lens. The videos were analyzed using ImageJ and MATLAB.[48]

The radius evolution of the capillary bridge and resulting liquid filament were used to determine extensional rheological properties. The solutions were observed to have two distinct regimes: (i) viscocapillary and (ii) elastocapillary. The viscocapillary regime is governed by the viscous and capillary stresses and is represented by the following equation[49]

$$\frac{R(t)}{R_0} = 0.0709 \frac{\sigma}{\eta R_0}(t_f - t) \tag{1}$$

where $R(t)$ is the radius of the fluid neck at the midpoint, R_0 is the radius of the nozzle, σ is the surface tension, η is η_0 or the zero-shear viscosity, t_f is the total pinch-off time, and t is the instantaneous time. The elastocapillary regime can best be represented by the equation from Entov and Hinch[50] with further development by McKinley et al.[51]

$$\frac{R(t)}{R_0} = \left(\frac{G_E R_0}{2\sigma}\right)^{1/3} \exp\left(-\frac{t}{3\lambda_E}\right) \tag{2}$$

where G_E is the elastic modulus and λ_E is the extensional relaxation time. Eqs 1 and 2 were fit to the radial evolution data by plotting $R(t)/R_0$ vs time and using linear regression for line fitting for the observed viscocapillary and elastocapillary regimes, which allowed for the determination of G_E and λ_E. Through the fit of the elastocapillary regime, the apparent extensional viscosity and extension rates could also be determined. The elastocapillary regime exhibits a uniform extensional flow with a rate

$$\dot{\varepsilon} = -2d \ln R(t)/dt \tag{3}$$

Through this, the extensional viscosity can be determined by the following formula[47]

$$\eta_E = \frac{\sigma}{\dot{\varepsilon}R} = \frac{\sigma}{-2dR(t)/dt} \tag{4}$$

The Hencky strain, or total accumulated strain, is shown to increase as $\varepsilon = 2\ln(R_0/R(t))$.

2.2.4. Electrospinning. The electrospinning apparatus was arranged in a parallel plate configuration with the plates 18–25 cm apart depending on the solvent. The system consisted of a syringe pump (Chemyx Inc. Fusion 100 dual syringe pump) and an ES30P-5W Gamma High Voltage Research power supply. The flow rate and voltage ranged from 0.3 to 1 mL/h and 15 to 20 kV, respectively, and were optimized for each polymer/solvent system such that a stable Taylor cone was formed and full solvent evaporation occurred. Spinning parameters remained constant at all concentrations. Experiments were conducted at room temperature (~23 °C) and unregulated relative humidity (54–60% RH). Samples were collected on aluminum foil and allowed to electrospin for at least 15 min. All samples were promptly stored in a desiccator until used for further characterization.

2.2.5. Morphology Characterization. Scanning electron microscopy (SEM) was performed using a Zeiss Ultra60 FE-SEM. Samples were sputtered with gold (Hummer 6) at a current of 15 mA for 1.5 min prior to evaluation.

3. RESULTS AND DISCUSSION

3.1. Electrospinning Regimes

In electrospinning, three distinct spinning regimes are seen typically corresponding to polymer concentration. The first regime occurs with semidilute polymer solutions where the concentration is greater than the critical coil overlap concentration (C^*) but less than the critical entanglement concentration (C_e), and there are no entanglements to form fibers, resulting in formation of beads/particles. When the solution concentration increases to greater than C_e, entanglements are introduced that lead to a beads-on-string morphology with beads connected by short fiber segments. Finally, when there are sufficient entanglements (about 2–3× critical entanglement concentration) to suppress the instabilities, smooth uniform fibers are produced, in what we call the heavily entangled or concentrated regime.[40,41] These regimes are consistent for nearly every polymer in electrospinning but occur at different concentrations. The regime

transitions can be determined for each polymer system through shear rheology and microscopic evaluation of fibers after electrospinning.

Electrospinning was performed for 55 kg/mol of PVP in MeOH, 1300 kg/mol of PVP in MeOH and water, 1000 kg/mol of PEO in water, and 145–180 kg/mol of PVA in water at a range of concentrations. Spinning conditions were kept constant for each polymer–solvent system. The resulting electrospun morphologies were examined with SEM, and full image analysis can be found in Figures S1–S5 in the SI. A list of concentrations corresponding to each morphology regime is shown in Table 1. Morphologies varied with concentration as

Table 1. Concentrations of Polymer Solutions (wt %) Corresponding to the Three Regimes Observed through SEM Morphology Analysis and the Concentration at Onset of Fiber Formation Divided by the Critical Entanglement Concentration

	beads	beads-on-string	fibers
1000 kg/mol PEO in water	<1	1–2.25	>2.25
145–180 kg/mol PVA in water	<2.5	2.5–6	>6
1300 kg/mol PVP in water	<14	14–25	>25
1300 kg/mol PVP in MeOH	<4	4–9	>9
55 kg/mol PVP in MeOH	<30	30–50	>50

expected, with beads seen at low concentrations and smooth fibers seen at higher concentrations for each polymer/solvent system analyzed. Fully uniform smooth fibers were determined when no beads could be observed on the sample surface. It should be noted that 1300 kg/mol of PVP in water resulted in smooth fibers at 25, 18, and 9 wt % in water, water with surfactant, and MeOH, respectively, which will be discussed later in this study. Increasing the concentration further above the transition from the beads-on-string to fiber regime resulted in an increase in the fiber diameter.

Traditionally, the morphology regimes have been correlated to the shear viscosity, specifically the changes in the slope of the relative viscosity vs concentration curve; therefore, shear viscosity was analyzed at varying concentrations, shown in Figure 2 for PEO and water and for all mixtures in Figures S6–
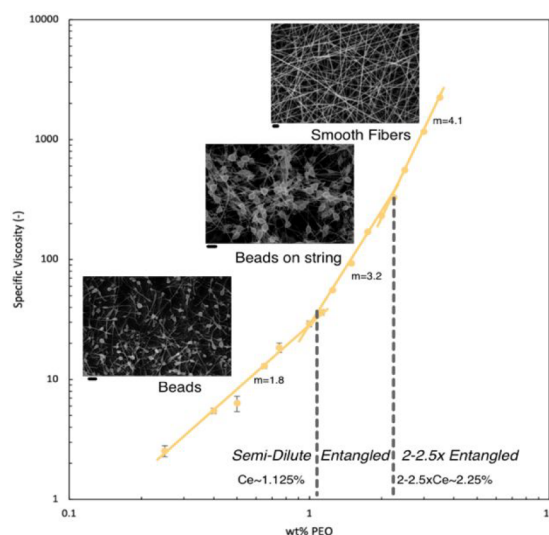
Figure 2. Specific viscosity vs concentration of PEO in water showing the three regimes with corresponding spinning morphologies.

Table 2. Experimentally Determined Values of Concentration, Shear Viscosity Measured at Low Shear Rates prior to Onset of Shear-Induced Rheological Behavior or Zero-Shear Viscosity (η_0), Surface Tension, Density, and Extensional Relaxation Time for Every Polymer in Each Regime[a]

	concentration (wt%)	polymer	density (g/mL)	η_0 (mPa·s)	surface tension (mN/m)	extensional relaxation time (ms)
beads/semidilute	0.75	PEO	1	17.3 ± 1.5	61.84	4.64 ± 0.16
	2	PVA	1.003	6.49 ± 0.45	55.27	-
	12	1300 kg/mol PVP–H_2O	1.018	197 ± 4.7	65.42	3.0 ± 0.4
	4	1300 kg/mol PVP–MeOH	0.802	10.3 ± 0.16	23.47	1.09 ± 0.39
	17	55 kg/mol PVP	0.832	4.48 ± 0.10	25.53	-
beads-on-string/ entangled	1.5	PEO	1	83.4 ± 8.4	61.63	7.90 ± 0.43
	4	PVA	1.006	31.3 ± 0.73	52.07	6.40 ± 1.5
	18	1300 kg/mol PVP–H_2O	1.026	739 ± 23	65.28	15.4 ± 3.5
	7	1300 kg/mol PVP–MeOH	0.810	30.7 ± 2.8	24.1	3.69 ± 0.51
	12	1300 kg/mol PVP–H_2O– surfactant	1.018	186 ± 4.9	32.75	1.49 ± 0.39
	30	55 kg/mol PVP	0.859	13.3 ± 0.42	24.74	0.382 ± 0.061
fibers/heavily entangled	2.25	PEO	1.001	293 ± 9.9	61.41	12.9 ± 1.2
	6	PVA	1.009	125 ± 3.4	51.6	14.6 ± 2.9
	25	1300 kg/mol PVP–H_2O	1.034	2820 ± 109	64.78	24.9 ± 4.7
	9	1300 kg/mol PVP–MeOH	0.815	53.8 ± 0.83	24.7	6.76 ± 0.33
	18	1300 kg/mol PVP–H_2O– surfactant	1.026	703 ± 25	29.87	4.68 ± 1.48
	50	55 kg/mol PVP	0.893	46.1 ± 2.32	24.61	1.47 ± 0.33

[a]Missing values were unable to be obtained reliably. Error for η_0 was obtained from 3 different solutions with 10 data points each. Error for extensional relaxation time was obtained from at least 8 separate runs.

S10 in the SI. The slope of relative viscosity plotted against concentration changes at the start of the entangled regime and heavily entangled regime, indicating the critical entanglement concentration and critical fiber formation concentration, respectively. The critical entanglement concentration was found to correspond to the transition from the beads to beads-on-string morphology, and the fiber formation transition was found to correspond to ~1.7–2.5× the critical entanglement concentration for all polymer systems, matching prior studies.[40] Though the slopes of the lines were not identical for each polymer system, in all cases, a large increase was seen at the critical entanglement concentration, and another small increase was seen at the critical fiber formation concentration.

The goal of this study is to understand how the solution elasticity needed to produce fibers changes with the solution properties, so we selected polymer concentrations in each solvent such that they were just within the regime of interest. The concentration chosen to represent the beads regime was chosen as a point slightly lower than the entanglement concentration in the semidilute regime, the beads-on-string regime was chosen at a point just above the entanglement concentration within the entangled regime, and the concentration for fibers was chosen at the onset of smooth fiber formation representing the heavily entangled regime. The specific values can be seen in Table 2 for each of the polymer solutions tested. By comparing samples in this way, we can study the effect of solvent and polymer properties on the elasticity needed to be in each morphology regime and develop an improved understanding of the electrospinnability.

3.2. Extensional Rheology

As previously studied, fiber formation in electrospinning is significantly influenced by the extensional rheological properties of the polymer solutions.[39] Here, we characterized the extensional rheology for the selected concentrations corre-

sponding to each regime. The radial decay of the capillary bridge was observed over time as shown in Figure 3 (data for
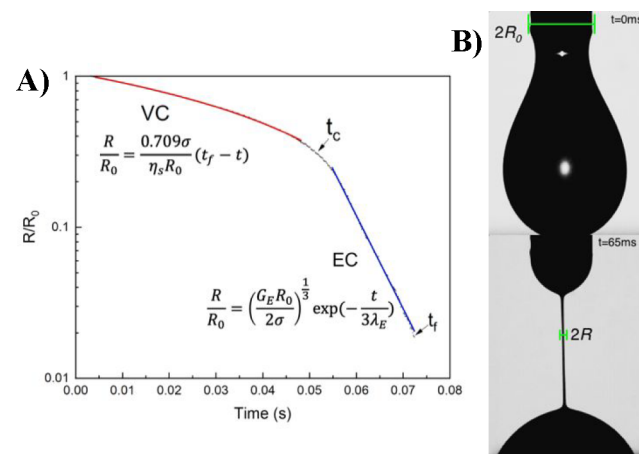

Figure 3. (A) Representative curve from 9 wt % PVP in methanol in the heavily entangled regime with viscocapillary (VC, red) and elastocapillary (EC, blue) governing equations and line fit of the elastocapillary regime. The radius evolution curve is on a semilog plot to accentuate the elastocapillary regime. (B) Still images obtained from video at $t = 0$ and $t = 65$ ms.

all solutions in SI section 3). The initial viscocapillary regime was seen by a linear decrease in radius over time as described by eq 1 and seen highlighted in red in Figure 3. Following the viscocapillary regime, the filament began to thin exponentially corresponding to an elastocapillary regime (seen in blue in Figure 3) typical of viscoelastic solutions. This regime was governed by eq 2. Through the data obtained from eqs 2–4, we were able to determine polymer extensional relaxation times and extensional viscosities. In the following sections, we use these values to examine the interplay between the elasticity

and the surface tension, concentration, and molecular weight in influencing the electrospinnability of each polymer solution.

Extensional relaxation times, shown in Table 2, varied across polymers and spinning regimes. The extensional relaxation time was found to increase significantly with polymer concentration with the range of relaxation times being 3.0–24.9 ms for 1300 kg/mol of PVP in water, 1.09–6.76 ms for 1300 kg/mol of PVP in MeOH, 0.382–1.47 ms for 55 kg/mol of PVP, 4.64–12.9 ms for PEO, and 6.4–14.6 ms for PVA. The relaxation times for solutions that formed smooth fibers were larger for higher-molecular-weight PVP than lower-molecular-weight PVP in methanol, 6.76 and 1.47 ms, respectively. This is likely due to greater chain stretching of the high-molecular-weight PVP. Though PEO and PVA have vastly different molecular weights, they exhibit similar relaxation times in both the beads-on-string and smooth fiber regimes, indicating that relaxation time is not solely dictated by chain length across different polymers.

Higher relaxation times indicate that the elastic component of viscoelastic behavior is observed for longer times; therefore, we see that greater polymer concentration leads to greater elasticity in solutions and additionally that the aqueous solutions we tested have observed greater elasticity. This is because the longer filament thinning times can allow for greater chain rearrangement and stretching. This was observed most clearly with 18 wt % PVP in H_2O with and without surfactant where the lower-surface-tension solution exhibited a lower relaxation time (specific comparison in SI Section 4). These effects can be further evaluated and related to the electrospinnability through dimensionless numbers such as the Deborah or Ohnesorge number, which will be discussed later.

Extensional viscosity can be computed using eq 4 for data in the elastocapillary regime. Since the extensional viscosity is a function of the strain in the filament, it is plotted vs Hencky strain as seen in Figure 4 (data for all solutions in SI Section 5). Extensional viscosity increases with increasing strain, signifying strain hardening behavior, which can stabilize the electrospinning jet and avoid breakup. Due to strain hardening, at sufficiently large strains, a terminal steady state extensional viscosity is reached, as be seen through a plateau at high

Hencky strain values. As it is difficult to quantitatively determine strain in the electrospinning jet, we cannot directly compare exact extensional viscosity values but rather examine values in the range of Hencky strain values observed in the elastocapillary regime.

In order to understand the impact of solvent properties on extensional viscosity required to form smooth fibers in more detail, we compared polymers in two solvents with vastly different surface tension values, MeOH and water (∼60 and 24 mN/m, respectively). As extensional viscosity is dependent on surface tension, seen in eq 4, extensional viscosity should increase with surface tension; however, to our knowledge, the interplay between surface tension and electrospinnability has not been studied through extensional rheology. Though surface tension is not the only element of the solvents that will impact the extensional viscosity and electrospinnability, we anticipate that the significant difference in surface tension of water and MeOH will lead to surface tension effects overwhelming others such as specific interactions of water with polymers, polymer chain conformation, etc. (Hansen solubility parameters and conductivities in Sections 6 and 7 of the SI). To further elucidate the surface tension effects, we additionally compared high-molecular-weight PVP in water (∼60 mN/m) to high-molecular-weight PVP in water with a surfactant, Triton X-100, (∼30 mN/m). The addition of surfactant maintains all other solution properties such as shear viscosity, conductivity, vapor pressure, and polymer solubility. By analyzing this data set, we see that the surface tension of the solution has a significant effect on the extensional viscosity required to electrospin fibers.

Surface tension values for every solution in each regime were obtained (Table 2), with solutions in water having surface tensions of 55–61 mN/m, solutions in MeOH having surface tensions of 23–25 mN/m, and the solution with surfactant having a surface tension of 30 mN/m. When comparing extensional viscosities in the beads-on-string and smooth fiber regimes (entangled and heavily entangled regimes, respectively), shown in Figure 4, we saw that the extensional viscosities of solutions with high surface tension (PEO, PVA, PVP in water) were consistently greater than those with low surface tension (low- and high-molecular-weight PVP in MeOH as well as PVP in water with surfactant). Some solutions in the beads or semidilute regimes did not have a strong enough viscoelastic response to display a clear elastocapillary regime; therefore, this regime was not fully studied.

In electrospinning, charge repulsion and elasticity are needed to overcome surface tension and fully suppress Rayleigh instabilities. Greater elasticity is needed to overcome higher-surface-tension forces, which in a low-elasticity solution would lead to bead formation. Fong et al. showed most simply that lowering the surface tension led to the formation of fibers through spinning, though they did not fully study the underlying driver of this.[38] Here, we showed that high-surface-tension solutions required higher extensional viscosity to form smooth fibers. This was most clearly seen when comparing the high-molecular-weight PVP in solutions with three different surface tensions: water (∼60 mN/m), methanol (∼24 mN/m), and water with surfactant (∼30 mN/m), where PVP in water requires a higher elasticity to spin uniform fibers (Figure 5) than the PVP in methanol or PVP in water with surfactant. PVP in water with surfactant produces smooth fibers at a lower concentration than PVP in pure water, since
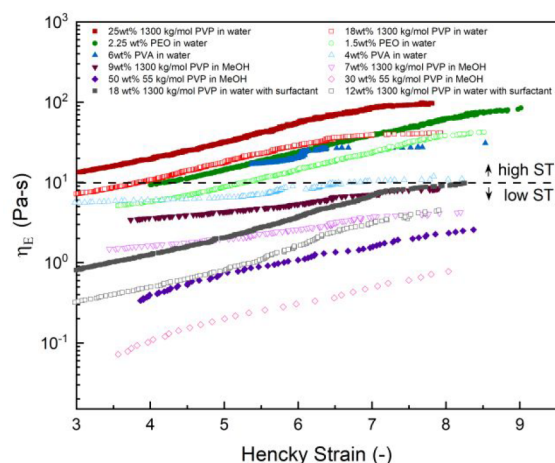
Figure 4. Extensional viscosity vs Hencky strain for beads-on-string/ entangled (open symbols) and fiber/heavily entangled (closed symbols) regimes; as seen, there is a clear difference in viscosities for corresponding strains for high-surface-tension (ST) solutions (water) vs low-surface-tension polymer solutions.
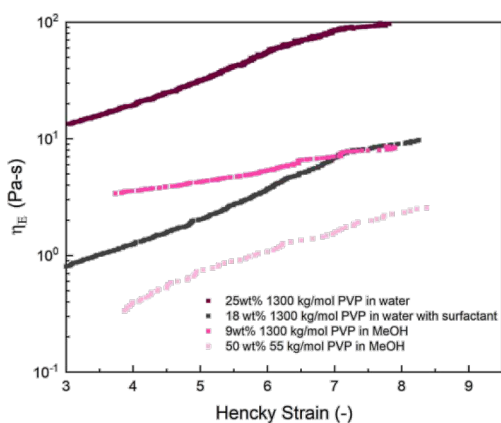
Figure 5. Extensional viscosity vs Hencky strain for all smooth fiber regime/heavily entangled PVP solutions including low- and high-molecular-weight PVP in MeOH and high molecular weight in MeOH, water, and water with surfactant.

the surface tension forces are lower. Interestingly, the terminal steady state extensional viscosities of PVP in MeOH and PVP in water with surfactant are nearly identical.

We further found that the requirement for high elasticity with high surface tension still holds when spinning 55 kg/mol of PVP in water; we were unable to produce smooth fibers with 55 kg/mol of PVP in water, as the elasticity needed to achieve fibers required concentrations so high we could not fully dissolve the PVP. Both water and MeOH are good solvents for PVP; therefore, we do not believe that excluded volume effects on the chain conformation and entanglements will have a significant impact on what we observe.

To confirm that the higher extensibility corresponds with the electrospinning regimes, as defined by the fiber morphology, we examine the rheology of different concentrations of otherwise identical polymer solutions in the three different spinning regimes. As seen in Figure 6, extensional viscosity increased with increasing concentration of PVP in water; this trend was seen with all polymers examined (shown in Figure S22). Between the beads and beads-on-string spinning regimes, we saw a large increase in the extensional viscosity, while we still saw a small increase between the beads-on-string and fiber regimes. This indicates that the increase in chain entanglements has a significant impact on extensibility as compared to unentangled polymers. To overcome the inertial forces and Rayleigh instabilities during electrospinning, the solution requires sufficient elasticity, which was provided here by the entanglements between polymer chains at high concentrations.

The molecular weight of the polymer is known to increase extensibility due to greater coil stretching in higher-molecular-weight polymers.[48] Longer polymer chains are able to stretch to a higher degree than shorter chains. Yu et al. also studied this effect in electrospinning for PEO/PEG solutions, but they did not directly compare extensional properties right at the onset of fiber formation for more than one molecular weight.[39] Much work has been done on how molecular weight affects spinnability, such as entanglement effects,[36] or how the coil−stretch transition affects fiber formation in dilute solutions.[52] We further investigated the effect of molecular weight on spinnability through the compared extensional viscosities of PVP at 55 and 1300 kg/mol in methanol at the onset of smooth fiber formation at 50 and 9 wt %, respectively (start of
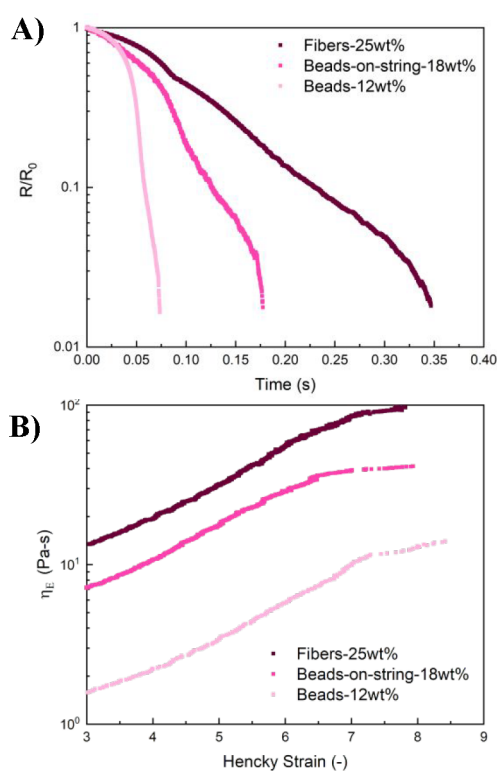

Figure 6. (a) Radius evolution data for PVP in water for each spinning regime. (b) Computed extensional viscosity vs Hencky strain for the corresponding radius evolution curves.

the heavily entangled regime). The higher-molecular-weight PVP had greater elasticity with higher extensional viscosity values for matched strain despite both solutions being at the critical concentration required for smooth fibers, as seen in Figure 5. This may be due to the onset of fiber formation occurring at $2.3 \times C_e$ for the 1300 kg/mol of PVP in methanol compared to $1.7 \times C_e$ for the 55 kg/mol of PVP, and thus, the 1300 kg/mol of PVP in methanol solution has a higher number of entanglements and a higher extensional viscosity. We will consider the potential reasons that 55 kg/mol of PVP requires fewer entanglements and a lower extensional viscosity to spin when discussing the *Oh* number in Section 3.3. Though molecular weight has an impact on extensibility, an examination of the 1300 kg/mol of PVP in water, methanol, and water with surfactant showed that the solvent, namely the solvent surface tension, has a more substantial impact on elasticity necessary to form smooth fibers than the molecular weight, with water leading to significantly higher extensional viscosities at the onset of fiber formation than water with surfactant or MeOH.

One solvent property that was not discussed thus far is the vapor pressure, despite the large differences between the water and MeOH vapor pressure. We did not study this parameter in detail, because it has been shown that in the steady jet region just past the Taylor cone, there is negligible solvent evaporation.[53] As this is the region where the bead formation occurs as well, solvent evaporation likely is not causing significant differences in fiber formation, and thus, vapor pressure is outside the scope of this study.

3.3. Dimensionless Numbers

To further understand solvent effects on fiber formation through elasticity, we compared each polymer solution in the

three regimes in terms of global dimensionless numbers. Dimensionless numbers in rheology can help us understand the relative importance of different forces acting on the solution during electrospinning. The inertial forces, which are driven by surface tension and lead to Rayleigh instabilities, compete with the viscous and elastic forces to determine the spinnability and fiber morphology. We characterized both the viscous to inertial and elastic to inertial effects, as polymer chain dynamics during spinning include both chain reptation during flow and chain stretching that can be observed by viscous and elastic effects respectively. The effects of these three forces can be characterized through three characteristic time scales, the inertial Rayleigh time, a viscous time scale, and a polymeric time scale. Studying the magnitude of viscous to inertial and elastic to inertial time scales allows for better understanding of whether the viscous or elastic effects in the fluid flows are more dominant. Higher viscous effects may indicate that chain entanglements are dominating the extensional rheology, whereas higher elastic effects may tell us that chain stretching has a greater effect; both play an important role in forming smooth fibers in electrospinning.

The Rayleigh time $t_R = (\rho R_0^3/\sigma)^{1/2}$ represents the time scale associated with the oscillation frequency of drop formation[54] and is a function of density, surface tension, and characteristic length scale, which in this case was the nozzle radius. We assume that the nozzle radius is a relevant characteristic length scale as the onset of instabilities and drop formation occurs nearly instantaneously at the needle tip. The droplets also thin at a similar rate; therefore, the initial diameter at the nozzle is used for simplicity. The viscous time scale, $t_v = \eta_0 R_0/\sigma$, depends on viscosity and surface tension, and the polymeric time scale can be represented by the relaxation time, which in this study was taken as the extensional relaxation time.

The ratio of t_v to t_R represents the Ohnesorge number (Oh), where $Oh = t_v/t_R = \eta_0/\sqrt{\rho\sigma R_0}$.[55] Oh characterizes the significance of viscous to inertial effects. An $Oh > 0.2$ has previously been shown to be sufficient for viscous forces to dominate inertial effects in viscoelastic filament thinning experiments.[56,57] Formenti et al. determined $Oh > 3$ in all of their spinnable solutions of nylon 6 in formic acid.[45] In our studies, we observed that smooth fibers were formed when $Oh > 0.35$ in MeOH solutions, as all spinnable solutions (highly entangled regime) had an Oh greater than 0.35, but water solutions did not exhibit a clear cutoff point, as seen in Figure 7a, though at smooth fiber formation, Oh was greater than 1. Since Oh is heavily influenced by the shear viscosity, we see that MeOH solutions consistently having lower η_0 exhibit lower Oh values. Therefore, Oh cannot be reliably used to predict electrospinnability without considering other solution properties.

We can, however, examine the difference in spinnability for the 1300 kg/mol of PVP and 55 kg/mol of PVP in methanol using the Oh number. At the concentration where these polymer solutions form fibers, the Oh number is ~0.2−0.3 for both solutions. The two solutions are both spinnable into fibers despite a significantly higher extensional viscosity for the 1300 kg/mol of PVP in methanol. This indicates that we can still spin the 55 kg/mol of PVP in methanol despite the low extensional viscosity, because it has very high viscous effects from the high concentration (50 wt %), leading to a η_0 similar to that of 1300 kg/mol of PVP in methanol (Table 2).
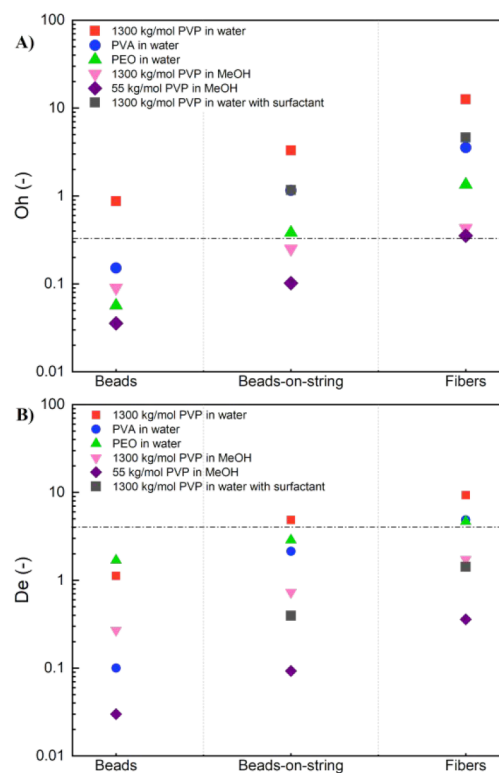

Figure 7. Oh (a) and De (b) evaluated in each spinning regime; dotted lines indicate Oh = 0.35 and De = 4.5, open symbols indicate water solutions, and closed symbols indicate MeOH solutions.

The ratio of extensional relaxation time to t_R corresponds to the Deborah number, which represents the ratio of elastic to inertial forces $De = \lambda_E/t_R = \lambda/\sqrt{\rho R_0^3/\sigma}$. $De > 1$ indicates that elastic forces dominate inertial forces. This is the more commonly studied dimensionless number for understanding electrospinnability. Yu et al. previously suggested that large De numbers (~6) are sufficient for fiber formation.[39] Khandavalli et al. determined that $De > 5$ produced smooth fibers for their system.[46] It should be noted that Yu used a different value for the characteristic length scale than Khandavalli and us. We found that all spinnable solutions in high-surface-tension solvents exhibited $De > 4.5$, seen in Figure 7b, but solutions in low-surface-tension solvents showed no trend for De, as the high-molecular-weight PVP in methanol in the beaded regime actually had a $De = 0.27$, whereas low-molecular-weight PVP in methanol in the fiber regime had a comparable of $De = 0.36$.

These results confirm the previously discussed need for complete suppression of inertial forces to produce smooth uniform fibers, by showing that either viscous forces or elastic forces dominate inertial forces in the heavily entangled regimes with Oh > 0.35 and $De > 1$. On the other hand, it suggests that suppression of forces can be driven by viscous or elastic forces. We showed that high-surface-tension solutions may require stronger elastic forces as seen through a higher De in the smooth fiber regime, whereas low-surface-tension solutions simply need strong viscous forces as seen through the high Oh numbers but low De numbers in the smooth fiber regime. This indicates that De could be used as an indicator for high-surface-tension solutions, whereas Oh can be used for low-surface-tension solutions with consideration of other solution factors such as η_0. Low-surface-tension solutions are not as heavily influenced by inertial forces; therefore, they do not need as

strong of viscous or elastic forces to obtain fibers in electrospinning. Weaker viscous forces are sufficient to suppress the inertial forces. Whereas, in high-surface-tension solutions when inertial forces are much greater, strong viscous and elastic forces from chain entanglements and chain stretching are necessary to promote fiber formation.

Though we found this in our systems, we do not believe this is a reliable way to determine spinnability more broadly, since it varies throughout solutions. We see an outlier with PVP in water in the entangled regime having a $De > 4.5$, yet uniform fibers were not observed. A more extensive study is required to prove whether either dimensionless number could be used to predict electrospinnability, as past literature and our studies all find different values at the point of smooth fiber formation.

4. CONCLUSION

This study shows that solvent surface tension has a strong effect on fiber formation in electrospinning where significantly higher elasticity is needed to promote smooth fiber formation in high-surface-tension solutions. This was determined by using DoS rheometry to study the extensional rheology of PEO, PVA, low-molecular-weight and high-molecular-weight PVP in water, water with surfactant, and MeOH at each spinning regime. The extensional relaxation time was found to increase with increasing polymer concentration with the longest relaxation time at 25 ms for high-molecular-weight PVP in water in the heavily entangled regime. We also showed that increased surface tension requires a higher polymer concentration and hence higher elasticity to suppress the Rayleigh instabilities driving droplet or bead formation, most notably observed through high-molecular-weight PVP being spun in solvents with three different surface tensions. The increased extensional viscosities observed for high-surface-tension solutions can further enhance the stability of the jet. Global dimensionless numbers may be a promising way to determine the electrospinnability with the observation that $De > 4.5$ for all high-surface-tension solutions and $Oh > 0.35$ in solutions with both low surface tension and low shear viscosity.

Through we note some limitations, this study provides a deeper understanding of the connection between solvent characteristics, viscoelasticity, and electrospinnability. We expect that this will enable the rational preparation of more complex spinning solutions being explored for technical applications in wearable electronics, pharmaceuticals, and more.

ASSOCIATED CONTENT

Supporting Information

The Supporting Information is available free of charge at https://pubs.acs.org/doi/10.1021/acspolymersau.1c00041.

> Fiber morphology images for all solutions; shear viscosity vs concentration analysis for all solutions; raw radius evolution figures including all runs for each concentration analyzed; additional in-depth comparison between PVP in water with and without surfactant; extensional viscosity figures for each solution; additional solution properties including conductivities and Hansen solubility parameters; alternative dimensionless number analysis; comparison of Trouton ratio for all solutions (PDF)

AUTHOR INFORMATION

Corresponding Author

Blair Brettmann − Materials Science and Engineering, Georgia Institute of Technology, Atlanta, Georgia 30332, United States; Chemical and Biomolecular Engineering, Georgia Institute of Technology, Atlanta, Georgia 30332, United States; orcid.org/0000-0003-1335-2120; Email: blair.brettmann@chbe.gatech.edu

Authors

Elena Ewaldz − Materials Science and Engineering, Georgia Institute of Technology, Atlanta, Georgia 30332, United States

Joshua Randrup − Chemical and Biomolecular Engineering, Georgia Institute of Technology, Atlanta, Georgia 30332, United States

Complete contact information is available at:
https://pubs.acs.org/10.1021/acspolymersau.1c00041

Author Contributions

Elena Ewaldz: Conceptualization, methodology, formal analysis, validation, investigation, writing−original draft, writing−review and editing, visualization. Joshua Randrup: methodology. Blair Brettmann: conceptualization, writing−review and editing, supervision, project administration, funding acquisition.

Notes

The authors declare no competing financial interest.

REFERENCES

(1) Faccini, M.; Vaquero, C.; Amantia, D. Development of Protective Clothing against Nanoparticle Based on Electrospun Nanofibers. *J. Nanomater.* **2012**, *2012*, 1−9.

(2) Yoon, B.; Lee, S. Designing Waterproof Breathable Materials Based on Electrospun Nanofibers and Assessing the Performance Characteristics. *Fibers Polym.* **2011**, *12* (1), 57−64.

(3) Sheng, J.; Zhao, J.; Yu, X.; Liu, L.; Yu, J.; Ding, B.; Ding, B. Chapter 17 - Electrospun Nanofibers for Waterproof and Breathable Clothing. *Electrospinning: Nanofabrication and Applications* **2019**, 543−570.

(4) Gharehaghaji, A. A. Nanotechnology in Sport Clothing. *Materials in Sports Equipment* **2019**, 521−568.

(5) Persano, L.; Camposeo, A.; Pisignano, D. Active Polymer Nanofibers for Photonics, Electronics, Energy Generation and Micromechanics. *Prog. Polym. Sci.* **2015**, *43*, 48−95.

(6) Chinnappan, A.; Baskar, C.; Baskar, S.; Ratheesh, G.; Ramakrishna, S. An Overview of Electrospun Nanofibers and Their

Application in Energy Storage, Sensors and Wearable/Flexible Electronics. *J. Mater. Chem. C* **2017**, 5 (48), 12657−12673.

(7) Ding, J.; Zhang, J.; Li, J.; Li, D.; Xiao, C.; Xiao, H.; Yang, H.; Zhuang, X.; Chen, X. Electrospun Polymer Biomaterials. *Prog. Polym. Sci.* **2019**, 90, 1−34.

(8) Katti, D. S.; Robinson, K. W.; Ko, F. K.; Laurencin, C. T. Bioresorbable Nanofiber-Based Systems for Wound Healing and Drug Delivery: Optimization of Fabrication Parameters. *Journal of Biomedical Materials Research - Part B Applied Biomaterials* **2004**, 70B (2), 286−296.

(9) Rim, N. G.; Shin, C. S.; Shin, H. Current Approaches to Electrospin Nanofibers for Tissue Engineering. *Biomedical Materials* **2013**, 8, 014102.

(10) Lannutti, J.; Reneker, D. H.; Ma, T.; Tomasko, D.; Farson, D. Electrospinning for Tissue Engineering Scaffolds. *Mater. Sci. Eng., C* **2007**, 27 (3), 504−509.

(11) Virji, S.; Huang, J.; Kaner, R. B.; Weiller, B. H. Polyaniline Nanofiber Gas Sensors: Examination of Response Mechanisms. *Nano Lett.* **2004**, 4 (3), 491−496.

(12) Senthamizhan, A.; Balusamy, B.; Uyar, T. Glucose Sensors Based on Electrospun Nanofibers: A Review Fiber-Based Platforms for Bioanalytics. *Anal. Bioanal. Chem.* **2016**, 408 (5), 1285−1306.

(13) Chinnappan, A.; Baskar, C.; Baskar, S.; Ratheesh, G.; Ramakrishna, S. An Overview of Electrospun Nanofibers and Their Application in Energy Storage, Sensors and Wearable/Flexible Electronics. *J. Mater. Chem. C* **2017**, 5 (48), 12657−12673.

(14) Ziabicki, A. *Fundamentals of Fibre Formation: the science of fibre spinning and drawing*; John Wiley and Sons: London, 1976.

(15) Han, C. D. A Theoretical Study on Fiber Spinnability. *Rheol. Acta* **1970**, 9 (3), 355−365.

(16) Lu, M.; Liao, J.; Gulgunje, P. V.; Chang, H.; Arias-Monje, P. J.; Ramachandran, J.; Breedveld, V.; Kumar, S. Rheological Behavior and Fiber Spinning of Polyacrylonitrile (PAN)/Carbon Nanotube (CNT) Dispersions at High CNT Loading. *Polymer* **2021**, 215, 123369.

(17) Ohta, Y.; Murase, H.; Sugiyama, H.; Yasuda, H. Non-Newtonian Rheological Behavior of Semi-Dilute Ultra-High Molecular Weight Polyethylene Solution in Gel-Spinning Process. 1: Concentration Effect on the Fundamental Rheological Properties. *Polym. Eng. Sci.* **2000**, 40 (11), 2414−2422.

(18) Pearson, J. R. A.; Shah, Y. T. Stability Analysis of the Fiber Spinning Process. *Trans. Soc. Rheol.* **1972**, 16 (3), 519−533.

(19) Hufenus, R.; Yan, Y.; Dauner, M.; Kikutani, T. Melt-Spun Fibers for Textile Applications. *Materials* **2020**, 13 (19), 4298.

(20) McKee, M. G.; Hunley, M. T.; Layman, J. M.; Long, T. E. Solution Rheological Behavior and Electrospinning of Cationic Polyelectrolytes. *Macromolecules* **2006**, 39 (2), 575−583.

(21) McKee, M. G.; Elkins, C. L.; Long, T. E. Influence of Self-Complementary Hydrogen Bonding on Solution Rheology/Electrospinning Relationships. *Polymer* **2004**, 45 (26), 8705−8715.

(22) Ewaldz, E.; Brettmann, B. Molecular Interactions in Electrospinning: From Polymer Mixtures to Supramolecular Assemblies. *ACS Applied Polymer Materials* **2019**, 1 (3), 298−308.

(23) Ding, J.; Zhang, J.; Li, J.; Li, D.; Xiao, C.; Xiao, H.; Yang, H.; Zhuang, X.; Chen, X. Electrospun Polymer Biomaterials. *Prog. Polym. Sci.* **2019**, 90, 1−34.

(24) Brettmann, B. K.; Cheng, K.; Myerson, A. S.; Trout, B. L. Electrospun Formulations Containing Crystalline Active Pharmaceutical Ingredients. *Pharm. Res.* **2013**, 30 (1), 238−246.

(25) Brettmann, B.; Bell, E.; Myerson, A.; Trout, B. Solid-State NMR Characterization of High-Loading Solid Solutions of API and Excipients Formed by Electrospinning. *J. Pharm. Sci.* **2012**, 101 (4), 1538−1545.

(26) Brettmann, B. K.; Myerson, A. S.; Trout, B. L. Solid-State Nuclear Magnetic Resonance Study of the Physical Stability of Electrospun Drug and Polymer Solid Solutions. *J. Pharm. Sci.* **2012**, 101 (6), 2185−2193.

(27) Persano, L.; Camposeo, A.; Pisignano, D. Active Polymer Nanofibers for Photonics, Electronics, Energy Generation and Micromechanics. *Prog. Polym. Sci.* **2015**, 43, 48−95.

(28) Deitzel, J.M; Kleinmeyer, J; Harris, D; Beck Tan, N.C The Effect of Processing Variables on the Morphology of Electrospun Nanofibers and Textiles. *Polymer* **2001**, 42 (1), 261−272.

(29) Thompson, C. J.; Chase, G. G.; Yarin, A. L.; Reneker, D. H. Effects of Parameters on Nanofiber Diameter Determined from Electrospinning Model. *Polymer* **2007**, 48 (23), 6913−6922.

(30) Zhang, S.; Shim, W. S.; Kim, J. Design of Ultra-Fine Nonwovens via Electrospinning of Nylon 6: Spinning Parameters and Filtration Efficiency. *Mater. Eng.* **2009**, 30 (9), 3659−3666.

(31) Theron, S. A.; Zussman, E.; Yarin, A. L. Experimental Investigation of the Governing Parameters in the Electrospinning of Polymer Solutions. *Polymer* **2004**, 45 (6), 2017−2030.

(32) Forward, K. M.; Rutledge, G. C. Free Surface Electrospinning from a Wire Electrode. *Chem. Eng. J.* **2012**, 183, 492−503.

(33) Shin, Y. M.; Hohman, M. M.; Brenner, M. P.; Rutledge, G. C. Experimental Characterization of Electrospinning: The Electrically Forced Jet and Instabilities. *Polymer* **2001**, 42 (25), 09955−09967.

(34) Tan, S. H.; Inai, R.; Kotaki, M.; Ramakrishna, S. Systematic Parameter Study for Ultra-Fine Fiber Fabrication via Electrospinning Process. *Polymer* **2005**, 46 (16), 6128−6134.

(35) Long, Y. Z.; Yan, X.; Wang, X. X.; Zhang, J.; Yu, M. Electrospinning. *Electrospinning: Nanofabrication and Applications* **2019**, 21−52.

(36) Rutledge, G. C.; Fridrikh, S. V. Formation of Fibers by Electrospinning. *Adv. Drug Delivery Rev.* **2007**, 59 (14), 1384−1391.

(37) Reneker, D. H.; Yarin, A. L. Electrospinning Jets and Polymer Nanofibers. *Polymer.* **2008**, 49, 2387−2425.

(38) Fong, H.; Chun, I.; Reneker, D. H. Beaded Nanofibers Formed during Electrospinning. *Polymer* **1999**, 40 (16), 4585−4592.

(39) Yu, J. H.; Fridrikh, S. V.; Rutledge, G. C. The Role of Elasticity in the Formation of Electrospun Fibers. *Polymer* **2006**, 47 (13), 4789−4797.

(40) Shenoy, S. L.; Bates, W. D.; Frisch, H. L.; Wnek, G. E. Role of Chain Entanglements on Fiber Formation during Electrospinning of Polymer Solutions: Good Solvent, Non-Specific Polymer−Polymer Interaction Limit. *Polymer* **2005**, 46 (10), 3372−3384.

(41) McKee, M. G.; Wilkes, G. L.; Colby, R. H.; Long, T. E. Correlations of Solution Rheology with Electrospun Fiber Formation of Linear and Branched Polyesters. *Macromolecules* **2004**, 37 (5), 1760−1767.

(42) Helgeson, M. E.; Grammatikos, K. N.; Deitzel, J. M.; Wagner, N. J. Theory and Kinematic Measurements of the Mechanics of Stable Electrospun Polymer Jets. *Polymer* **2008**, 49 (12), 2924−2936.

(43) Hodgkinson, T.; Chen, Y.; Bayat, A.; Yuan, X. F. Rheology and Electrospinning of Regenerated Bombyx Mori Silk Fibroin Aqueous Solutions. *Biomacromolecules* **2014**, 15 (4), 1288−1298.

(44) Wang, M.; Hsieh, A. J.; Rutledge, G. C. Electrospinning of Poly(MMA-Co-MAA) Copolymers and Their Layered Silicate Nanocomposites for Improved Thermal Properties. *Polymer* **2005**, 46 (10), 3407−3418.

(45) Formenti, S.; Castagna, R.; Momentè, R.; Bertarelli, C.; Briatico-Vangosa, F. The Relevance of Extensional Rheology on Electrospinning: The Polyamide/Iron Chloride Case. *Eur. Polym. J.* **2016**, 75, 46−55.

(46) Khandavalli, S.; Sharma-Nene, N.; Kabir, S.; Sur, S.; Rothstein, J. P.; Neyerlin, K. C.; Mauger, S. A.; Ulsh, M. Toward Optimizing Electrospun Nanofiber Fuel Cell Catalyst Layers: Polymer-Particle Interactions and Spinnability. *ACS Applied Polymer Materials* **2021**, 3 (5), 2374−2384.

(47) Dinic, J.; Jimenez, L. N.; Sharma, V. Pinch-off Dynamics and Dripping-onto-Substrate (DoS) Rheometry of Complex Fluids. *Lab Chip* **2017**, 17 (3), 460−473.

(48) Dinic, J.; Biagioli, M.; Sharma, V. Pinch-off Dynamics and Extensional Relaxation Times of Intrinsically Semi-Dilute Polymer Solutions Characterized by Dripping-onto-Substrate Rheometry. *J. Polym. Sci., Part B: Polym. Phys.* **2017**, 55, 1692−1704.

(49) Papageorgiou, D. T. On the Breakup of Viscous Liquid Threads. *Phys. Fluids* **1995**, 7 (7), 1529−1544.

(50) Entov, V. M.; Hinch, E. J. Effect of a Spectrum of Relaxation Times on the Capillary Thinning of a Filament of Elastic Liquid. *J. Non-Newtonian Fluid Mech.* **1997**, *72* (1), 31−53.

(51) McKinley, G. H.; Spiegelberg, S. H.; Anna, S. L.; Yao, M. Extensional Rheometry of Polymer Solutions and the Uniaxial Elongation of Viscoelastic Filaments. *Fourth Microgravity Fluid Physics & Transport Phenomena Conference* **1998**, 504−509.

(52) Malkin, A. Y.; Semakov, A. V.; Skvortsov, I. Y.; Zatonskikh, P.; Kulichikhin, V. G.; Subbotin, A. V.; Semenov, A. N. Spinnability of Dilute Polymer Solutions. *Macromolecules* **2017**, *50* (20), 8231−8244.

(53) Stephens, J. S.; Frisk, S.; Megelski, S.; Rabolt, J. F.; Chase, D. B. 'Real Time'" Raman Studies of Electrospun Fibers. *Appl. Spectrosc.* **2001**, *55* (10), 1287−1290.

(54) Rayleigh, L. On the Stability, or Instability, of Certain Fluid Motions. *Proceedings of the London Mathematical Society* **1879**, *s1−11* (1), 57−72.

(55) McKinley, G. H.; Renardy, M. Wolfgang von Ohnesorge. *Phys. Fluids* **2011**, *23* (12), 127101.

(56) Clasen, C.; Phillips, P. M.; Palangetic, L.; Vermant, J. Dispensing of Rheologically Complex Fluids: The Map of Misery. *AIChE J.* **2012**, *58*, 3242−3255.

(57) Campo-Deaño, L.; Clasen, C. The Slow Retraction Method (SRM) for the Determination of Ultra-Short Relaxation Times in Capillary Breakup Extensional Rheometry Experiments. *J. Non-Newtonian Fluid Mech.* **2010**, *165* (23−24), 1688−1699.